Wiley
Advances in Civil Engineering
Volume 2024, Article ID 4853773, 16 pages
https://doi.org/10.1155/2024/4853773

WILEY

Research Article

Data-Driven Method for Probabilistic Response Prediction of Cable-Stayed Bridges

Minsun Kim,[1] Jaebeom Lee,[2] Kyoung-Chan Lee,[3] Jeong Hwan Jang,[4] and Young-Joo Lee[1]

[1]*Department of Civil, Urban, Earth, and Environmental Engineering, Ulsan National Institute of Science and Technology (UNIST), UNIST-gil 50 44919, Ulsan, Republic of Korea*
[2]*Division of Physical Metrology, Korea Research Institute of Standards and Science, Gajeongro 267 34113, Daejeon, Republic of Korea*
[3]*Department of Civil and Railroad Engineering, Pai Chai University, Baejaero 155-40 35345, Daejeon, Republic of Korea*
[4]*TM E&C, 1005, Seongnam Central Biz Tower 1, 314, Galmahi-ro, Jungwon-gu, Seongnam-si, Gyeonggi-do, Republic of Korea*

Correspondence should be addressed to Young-Joo Lee; ylee@unist.ac.kr

Received 18 April 2024; Accepted 10 June 2024

Academic Editor: Thanh-Canh Huynh

This study proposes a data-driven method for predicting the probabilistic response of cable-stayed bridges. The proposed method is used to construct an optimal prediction model based on a data-driven machine-learning method. In addition, the accuracy and efficiency of the prediction model are improved by considering the correlation coefficients between the input sensor data and the output of the target response. The proposed method is comprised of two steps: the selection of meaningful features and the construction of a probabilistic prediction model employing Gaussian process regression. The proposed method is applied to an in-service cable-stayed bridge in the Republic of Korea using actual measurement data from various sensors. For comparison purposes, two parametric studies are performed, and the effects of the proposed feature-selection procedure are investigated based on the normalized correlation coefficients. Consequently, the proposed feature-selection method is proven to increase the accuracy and efficiency of the prediction.

1. Introduction

Structural health monitoring (SHM) can be used to evaluate structural conditions in real time and has been applied to monitor the structural safety of bridges based on measurement data [1]. For example, Liu et al. [2] assessed the structural performance of a bridge at the system level using SHM. Agdas et al. [3] attempted to identify structural damage through visual inspection and provided a decision-making framework based on SHM. To improve the real-time performance of such tasks, previous studies developed smart sensor technologies [4, 5, 6]. These studies have demonstrated that SHM provided an efficient method for the long-term monitoring of structural characteristics, such as the force, strain, displacement, and vibration of a bridge.

As cable bridges (e.g., cable-stayed and suspension bridges) are considered crucial civil infrastructures, SHM techniques have been applied to monitor their structural conditions and identify abnormal responses in real-time using measurement data obtained from various sensors. Jang et al. [4] presented a wireless smart sensor network deployed in an actual cable-stayed bridge and evaluated its performance using several methods. Haji Agha Mohammad Zarbaf et al. [7] proposed a new methodology based on a genetic algorithm and particle swarm optimization to estimate cable tension forces, which are critical structural components that need to be monitored for a cable-stayed bridge.

Recent studies have focused on identifying structural damage and anomalies in cable-stayed bridges using measurement data. Anomaly detection involves identifying patterns in data that deviate from expected behavior [8]. To assess structural conditions based on measurement data, it is important to set accurate thresholds for detecting abnormal or unusual behaviors [9]. Huynh et al. [10]

conducted the structural identification for a cable-stayed bridge under a typhoon using the measurement data. Additionally, structural identification of the bridge was conducted at various wind speeds to assess the changes in the bridge's dynamic characteristics caused by the typhoon. Mehrabi and Farhangdoust [11] assessed the cable responses using a laser-based vibration technique for health monitoring of cable-supported structures. Similarly, several researchers conducted the structural identification of cable-supported structures using the measurement data from various sensors, to detect abnormal or unusual responses [12, 13, 14, 15].

Therefore, prediction models related to artificial intelligence (AI) techniques have been employed to set these thresholds and detect anomalies based on measurement data. For example, Lee et al. [16] presented a methodology for monitoring structural responses through a pattern analysis of measurement data and employed an autoregression model for predicting structural responses. This method detected anomalous responses when specific measurement data deviated from the predicted pattern, serving as a threshold for anomaly detection. Furthermore, Pamuncak et al. [17] proposed a method for predicting the cable forces of cable-stayed bridges using temperature data as input, employing a convolutional neural network (CNN), which is a deep learning technique. By using a prediction model based on data-driven approaches, the prediction of structural response was utilized to detect damage or abnormal responses in cable-stayed bridges [17, 18]. However, most studies have utilized deterministic machine-learning models for the response prediction of cable-stayed bridges and suspension bridges [18, 19, 20].

When constructing machine-learning models for predicting responses, it is often necessary to consider uncertainty related to measurement data. It can be challenging to reduce the uncertainty of the measurement data despite the increasing amount of available data [21]. To address this issue, several researchers have utilized probabilistic methods to consider the uncertainty of measurement data. For example, Lee et al. [22] proposed a new probabilistic method based on Gaussian process regression (GPR) that provided both the prediction interval and predictive mean. In addition, the method was used for decision-making regarding bridge maintenance by utilizing the results of the predictive interval and prediction mean obtained through the GPR. Wang et al. [23] employed GPR to predict the strain of a suspension bridge during typhoon events. Previous studies have proposed methods for probabilistic response prediction, considering the influence of environmental factors (e.g., temperature and wind) on the responses of structures. However, these studies did not include a process for selecting environmental data that exhibited a high correlation with the predicted responses of structures to reduce the complexity of the model. Using all available data, including less-correlated data, to construct a predictive model leads to reduced prediction accuracy and increased computational time.

Cable-stayed bridges typically have a relatively large number of sensors that measure various physical quantities related to the environmental and structural responses. However, the prediction becomes inaccurate and ineffective if a prediction model is constructed on the basis of a dataset that includes irrelevant and redundant data. High-dimensional data analysis is required, which subsequently increases the complexity of the prediction model. According to Saunders et al. [24], irrelevant and redundant data can deceive the algorithm, thus increasing model error. Similarly, Cai et al. [25] proposed enhancing the quality of measurement data. This can increase the accuracy of a machine-learning model and reduce the required learning time by reducing the dimensionality of the data [26]. Blum and Langley [27] described several important definitions of relevance and proposed a feature-selection algorithm for selecting relevant features. Moreover, they characterized feature-selection methods as embedded, filter, and wrapper approaches [28]. Although these approaches have the advantage of selecting optimal feature subsets, they have limitations related to selecting suboptimal feature subsets, large time costs, and the selection of machine-learning models [29, 30]. Thus, subsequent studies have proposed hybrid models that combined the filter, wrapper, and embedded approaches to overcome these disadvantages [31, 32, 33, 34, 35].

For this reason, when performing response prediction for cable-stayed bridges using various measurement data, it should consider addressing the model complexity due to high-dimensional data. Fang et al. [36] suggested surrogate models based on support vector regression, artificial neural network, and GPR for the response prediction of a cable-stayed bridge and utilized a machine-learning model to consider the correlation between the input and target (i.e., structural response) data. In the study, the proposed method improved the accuracy and efficiency of machine-learning models for response prediction. However, this surrogate model required a complex process to calculate the optimal prediction using various machine-learning models. Therefore, this study proposes a method for feature selection to improve the accuracy and efficiency of prediction models using a hybrid approach. In addition, the proposed method integrates filter and wrapper approaches and enables the construction of an optimal prediction model based on a new index. This new index considers the correlation between input (i.e., environmental data) and output (i.e., target response) data based on the normalized correlation coefficient for the selection of relevant feature subsets.

2. Proposed Method

To predict the cable responses of a cable-stayed bridge effectively, it is important to construct an optimal prediction model with improved accuracy and efficiency while considering the correlation among multiple measurement data. The proposed method comprises two steps: feature selection and construction of the prediction model. In the first step, only the data related to the bridge response to be predicted are selected from the large amount of input data obtained from the various sensors of a cable-stayed bridge. In the second step, the selected data are applied to GPR to construct a response prediction model.

In the feature-selection step, only the data related to the predicted target information are systematically selected based on the correlation between the input and output datasets. For the task, this study introduces a normalized index based on the Pearson correlation coefficient (hereafter referred to as the correlation coefficient) and sets the criteria for feature selection. This index denotes the absolute value of the correlation coefficient between the input and output data. Based on this, feature selection can be performed according to equivalent criteria for datasets obtained from various sensors. When relevant datasets are selected, a probabilistic prediction model is constructed using GPR. For new input data, the constructed GPR model provides not only the predictive mean but also the standard deviation. In addition, the predictive model analysis can be repeated to determine the optimal criterion that resumes the process of feature selection. These two steps are described in Sections 2.1 and 2.2 along with their theoretical backgrounds.

2.1. Feature Selection Based on Z-Index. A cable-stayed bridge is often equipped with various types of sensors for monitoring its structural health. In this study, measurement datasets from various sensors are utilized to predict the tension forces of cables. A cable-stayed bridge is a system comprised of several structural components; thus, its sensor datasets need to be correlated at a certain level. When predicting the response of a specific structural component, the prediction accuracy can be increased by considering the correlated sensor data. However, the data from other sensors may have a low correlation with the target structural response. Nonetheless, the prediction accuracy can be reduced and the computational time increased if all available data, including less-correlated data, are applied to construct a predictive model. Therefore, it is critical to select the input data related to the target structural response from among various measurement datasets.

Two methods are often adopted to improve the accuracy of predictive models: feature selection and feature extraction [37]. Feature selection is the process of selecting the best feature among all features, that is, the one that satisfies various criteria defining relevance. Thus, feature selection focuses on the selection of relevant features from existing data. In feature extraction, new features are created by combining existing features. Feature extraction focuses on making features of the original data useful.

Saunders et al. [24] suggested an approach for feature selection based on the reduced dimensionality of data, aiming at the computational efficiency and accuracy of a machine-learning model. In the research, feature selection was applied to simplify the construction of the model, and relevant features were selected. In other words, the approach increased accuracy in a model with fewer data than the original data points. In addition, reducing the complexity of the learning results enhanced the understanding of the underlying process.

Several researchers showed that feature selection enabled the effective construction of a regression model for accurate prediction [27, 28, 29]. However, feature selection often requires a selection criterion. As it was found that, for a target cable-stayed bridge, the temperature and wind speed (i.e., input data) were correlated to the cable tension force (i.e., output data), this study introduces correlation coefficients between the input and output data for feature selection. The correlation coefficient of a dataset is a measure of the linear correlation between two sets of data. It has a value between −1 and 1, with the absolute value indicating that the linear equation completely describes the relationship between the input and output (i.e., with all data points lying on a line). In contrast, there is no linear dependency between the variables when the correlation coefficient is zero. Therefore, the absolute value of the correlation coefficient can be introduced as a criterion to determine relevant features. This study selects the input data with the criterion being the absolute value of the correlation coefficient between the input and output data. Subsequently, the selected input data are used to establish a machine-learning model by employing GPR to predict the structural response.

However, input features may not be selected properly when the correlation coefficients with inputs vary by output. Figure 1 shows an example of the correlation coefficient matrix for the eight input and five output datasets. If feature selection is performed for relevant data based on the correlation coefficient, it involves setting different threshold values for the selection of relevant input data related to each output datum. For example, when y_1, which is generally highly correlated with the input data, is designated with a threshold value of 0.5, the data of x_3, x_5, x_6, and x_8, which have an absolute value of the correlation coefficient over the threshold value, are selected as features. On the other hand, when y_2, which is generally less correlated with the input data, is designated with the same threshold value, no input data can be selected. To select a similar number of datasets for y_2, a smaller threshold value needs to be set. For example, when y_2 is designated with a threshold value of 0.2, the data of x_5, x_6, and x_7 are selected as input features. In other words, if the same threshold value is designated to predict all output data, this may result in an excessive or insufficient amount of input data, which may decrease prediction accuracy and efficiency. Therefore, it is difficult to select an appropriate number of input data due to the inconsistent level of correlation coefficients between input and output data.

To resolve this issue, in this study, normalizing the absolute values of the correlation coefficients and setting a threshold value is proposed. For normalization, the Z-score can be adopted [38, 39, 40, 41]. Z-score normalization facilitates the identification of the relative importance of the correlation to the overall correlation. The index transformed into a relative correlation between the input and output data is denoted as the Z-index, which indicates the normalized importance of each correlation coefficient between the input and output data in the entire dataset. Feature selection is used to configure the criteria for selecting the relevant input data using the Z-index as follows:

$$\mathrm{Z}_j = \frac{\left|\rho_{i,j}\right| - \left|\rho_j\right|_{\mathrm{mean}}}{\left|\rho_j\right|_{\mathrm{std}}}, \tag{1}$$

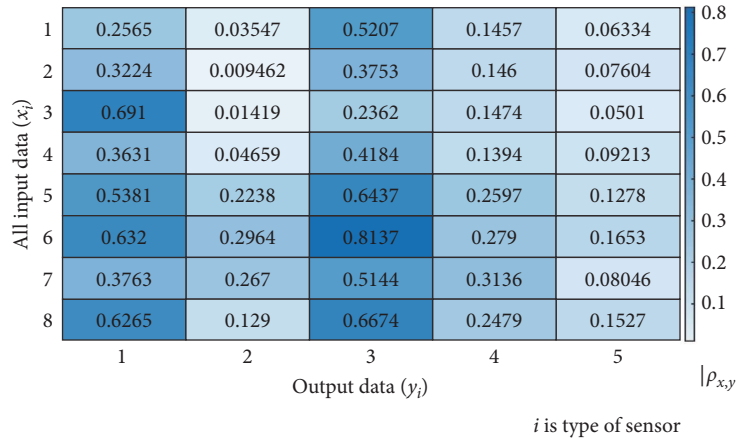

FIGURE 1: Feature selection according to the correlation coefficient.

where i and j denote the number of vectors for the input and output data, respectively, and $|\rho_{ij}|$ denotes the absolute value of the correlation coefficient calculated according to the vectors of the ith input and jth output. $|\rho_j|_{\text{mean}}$ denotes the mean of the absolute value in the vector of the jth output, and $|\rho_j|_{\text{std}}$ denotes the standard deviation of the absolute value in the output data vector. Equation (1) can be used to select a feature (i.e., input data), which can be represented as a change $|\rho_{x,y}|$ to Z_i in Figure 1.

2.2. Prediction Model Construction Using GPR. A Gaussian process is a stochastic process that can be defined as a collection of random variables, and it is assumed that all data follow a multivariate normal distribution [42]. This is described as the Gaussian process assumption, and GPR uses an inference regarding the predicted value based on this assumption [22]. GPR is also categorized as a machine-learning method based on the Bayesian theory [43], and more details can be found in Lee et al. [22] and Rasmussen [42].

The measurement data of the obtained sensors can be used to perform GPR for prediction. Equation (2) describes a noisy training dataset **D** comprised of a training input matrix **X** and training output vector **y**:

$$\mathbf{D} = \{(\mathbf{X}, \mathbf{y})\} = \{(x_{i,j}, y_i) | i = 1, \ldots, N; j = 1, \ldots, T\}, \tag{2}$$

where $x_{i,j}$ denotes the component of the training input matrix **X**, and y_i denotes the component in the training output vector **y**, which have the sizes of $N \times T$ and $N \times 1$, respectively. Subsequently, the prediction of the Gaussian mean and variance of the output are determined based on the assumptions of Gaussian processes.

Equation (3) describes the relationship between the input and output data using a regression function and observation error vector:

$$\mathrm{y} = f(\mathbf{X}) + \varepsilon, \tag{3}$$

where $f(\cdot)$ denotes the regression function of **X**, and $\boldsymbol{\varepsilon}$ denotes the error vector. The errors of the observation are assumed to comprise an independent and identically distributed Gaussian distribution with a zero mean and constant variance of the noise, indicated as $N(0, \sigma^2_n \mathbf{I})$. The regression function $f(\cdot)$ is assumed to have a Gaussian distribution with a zero-mean and covariance function $\mathbf{K}(\cdot,\cdot)$, which is expressed as follows:

$$f(\mathbf{X}) \sim gp(\mathbf{O}, \mathbf{K}(\mathbf{X}, \mathbf{X}')). \tag{4}$$

For prediction purposes, the test input matrix $\mathbf{X}_*$ is measured to estimate the test output vector $\mathbf{y}_*$ using the Bayes rule. The multivariate Gaussian variables are expressed as follows:

$$\begin{bmatrix} f(\mathbf{X}) \\ f_*(\mathbf{X}_*) \end{bmatrix} = N\left(\mathbf{O}, \begin{bmatrix} \mathbf{K}(\mathbf{X}, \mathbf{X}) & \mathbf{K}(\mathbf{X}, \mathbf{X}_*) \\ \mathbf{K}(\mathbf{X}_*, \mathbf{X}) & \mathbf{K}(\mathbf{X}_*, \mathbf{X}_*) \end{bmatrix}\right), \tag{5}$$

where $f_*(\cdot)$ denotes the regression function of $\mathbf{X}_*$, which is expressed as a Gaussian distribution. **K** (**X**, **X**) denotes the covariance matrix of the training input matrix **X**, **K** (**X**, $\mathbf{X}_*$) denotes the covariance matrix between the training inputs **X**

and test inputs $\mathbf{X}_*$, K ($\mathbf{X}_*$, $\mathbf{X}$) denotes $\mathbf{K}$ ($\mathbf{X}_*$, $\mathbf{X}$)$^{\mathrm{T}}$, and $\mathbf{K}$ ($\mathbf{X}_*$, $\mathbf{X}_*$) denotes the covariance matrix of the test input matrix $\mathbf{X}_*$. However, noise exists in the training data shown in Equation (3), as well as in the test data. Therefore, the noise variance $\sigma^2{}_n$ is added in the covariance matrix as follows:

$$\begin{bmatrix} \mathbf{y} \\ \mathbf{y}_* \end{bmatrix} \Bigg| \mathbf{X}, \mathbf{X}_* = \begin{bmatrix} f(\mathbf{X}) \\ f_*(\mathbf{X}_*) \end{bmatrix} + \begin{bmatrix} \varepsilon \\ \varepsilon_* \end{bmatrix} = N\left(\mathbf{O}, \begin{bmatrix} \mathbf{K} + \sigma_n^2\mathbf{I} & \mathbf{K}_* \\ \mathbf{K}_*^{\mathrm{T}} & \mathbf{K}_{**} \end{bmatrix}\right), \tag{6}$$

where $\mathbf{O}$ denotes the zero matrix, and $\mathbf{K}$, $\mathbf{K}_*$, $\mathbf{K}^{\mathrm{T}}{}_*$, and $\mathbf{K}_{**}$ are indicated as $\mathbf{K}$ ($\mathbf{X}$, $\mathbf{X}$), $\mathbf{K}$ ($\mathbf{X}$, $\mathbf{X}_*$), $\mathbf{K}$ ($\mathbf{X}_*$, $\mathbf{X}$)$^{\mathrm{T}}$, and $\mathbf{K}$ ($\mathbf{X}_*$, $\mathbf{X}_*$), respectively. Therefore, the predictive mean and covariance are expressed as follows:

$$\mathbf{y}_* | \mathbf{y}, \mathbf{X}, \mathbf{X}_* \sim N(\mathbf{K}_*^{\mathrm{T}}(\mathbf{K} + \sigma_n^2\mathbf{I})^{-1}\mathbf{y}, \mathbf{K}_{**} - \mathbf{K}_*^{\mathrm{T}}(\mathbf{K} + \sigma_n^2\mathbf{I})^{-1}\mathbf{K}_*). \tag{7}$$

In this study, the automatic relevance determination (ARD) kernel function is adopted for multidimensional inputs, as follows:

$$k(\mathbf{x}_p, \mathbf{x}_q|\theta) = \theta_2^2 \exp\left[\frac{1}{2}\sum_{m=1}^{d}\frac{(\mathbf{x}_p - \mathbf{x}_q)^2}{\theta_1^2}\right], \tag{8}$$

where $\mathbf{x}_p$ and $\mathbf{x}_q$ denote the input vectors of the pth and q, respectively. The hyperparameter θ (as related to the accuracy of a covariance matrix) can indicate θ_1 and θ_2 in the case of the ARD kernel function. In addition, θ_1 denotes the characteristic length scale of the dimension and θ_2 denotes the signal standard deviation. Using the ARD kernel function, the relevance of the input feature can be determined based on θ_1 [44].

2.3. Proposed Method Integrated with Feature Selection and Prediction Model Construction. Figure 2 shows a flowchart of the proposed method. It requires an iterative procedure with varying threshold values of the Z-index, and each iteration consists of two steps: input data selection (i.e., feature selection) and prediction-model construction. The input and output data are collected during initialization, and $|\rho_{ij}|$ is calculated for the ith input and jth output. Consequently, a correlation coefficient matrix, such as that shown in Figure 1, can be constructed for the entire dataset. Additionally, the first threshold value of the Z-index is determined using its predetermined minimum value ($Z_{\min}$). Next, $|\rho_j|_{\mathrm{mean}}$ and $|\rho_j|_{\mathrm{std}}$ are calculated for the jth output, and Z_{ij} is calculated for ith input and jth output. Consequently, a Z-index coefficient matrix is constructed for the entire dataset.

Subsequently, for the jth output, the input data that satisfy $Z_{ij} \geq Z_{\mathrm{th}}$ are selected. The selected input data are considered relevant to the target output (i.e., jth output) based on the given threshold value of the Z-index (i.e., Z_{th}). When the relevant input data are selected, a probabilistic prediction model is constructed using GPR, and the prediction error is calculated for the test data. This procedure is repeated until Z_{th} exceeds a given maximum value (i.e., $Z_{\max}$) or no input data are selected for any of the output data; Z_{th} is incremented by α each time. When the iterative procedure is terminated, the best threshold value of the Z-index is determined as the one with the minimum prediction error. More details of the flowchart are provided in Section 3 with an example application.

3. Application Example

3.1. Target Cable-Stayed Bridge and Sensing Data. To test the proposed method, it is applied to the 2nd Jin-do Bridge, an actual cable-stayed bridge connecting Jindo Island and Haenam Province in the Republic of Korea. The bridge was constructed in 2005 as an addition to the existing Jin-do Bridge. It is a three-span steel-box girder cable-stayed bridge with a midspan of 344 m, side spans of 70 m each, and a width of 12.2 m. The steel-box girder is supported by 60 steel parallel wire strand cables, and all stayed cables are connected to two A-shaped steel pylons on the concrete piers [5, 45].

In Yang et al.'s [46, 47] previous studies, the relationship between environmental factors and structural responses of cable-stayed bridges was investigated. Similar to these studies, this study incorporates data collected from the thermometers and anemometers as input data and uses the measurement data of the cable tension forces as output data. The locations of the sensors on the bridge are shown in Figure 3.

Four thermometers are located on each section of the two pylons (i.e., TMP001_1–TMP001_4 and TMP003_1–TMP003_4), and seven sensors are placed on a section of the central girder (i.e., TMP002_1–TMP002_7). In addition, anemometers are located with a sensor on the pylon in the direction of Jin-do (i.e., WGT001) and at the center of the girder (i.e., WGT002). The anemometer has two channels: wind speed and wind direction. The cable accelerometers (CAC001-17) are located on 17 stayed cables arranged in pairs. For example, CAC001 and CAC002 are located on stayed cables from the left and right sides, respectively, in the direction of the bridge axis. The tension force data of the stayed cables are obtained using an accelerometer via a vibration method [48, 49].

All datasets (i.e., temperature, wind speed, wind direction, and cable tension force) were recorded for 5 weeks from March 16 to April 12, 2019. In this example, the data for the first 4 weeks are used as training data to construct a GPR model, and the remaining weekly dataset is used as test data. The dataset consists of 144 data points for 1 day; thus, the training and testing datasets are comprised of 4,032 and 1,008 data points, respectively.

3.2. Performance Assessment of Predictive Mean. The mean absolute percentage error (MAPE) is considered for the performance assessment of the predictive mean. The root mean square error (RMSE), which is widely used to quantify errors, is known to be highly dependent on the data size [50]. Kim and Kim [51] stated that the MAPE had the advantage of scale independence because it was based on a ratio, whereas

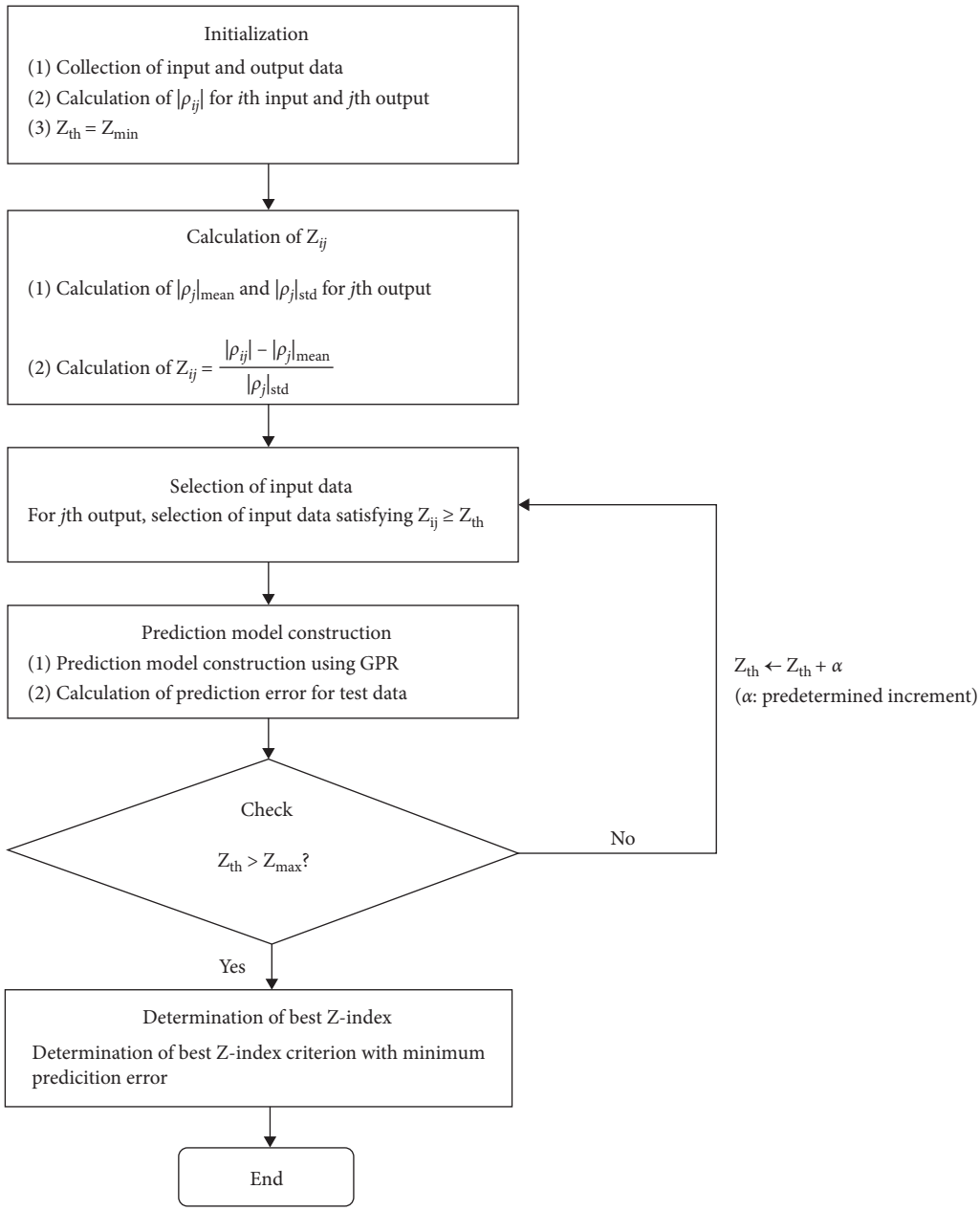

Figure 2: Flowchart of proposed method.

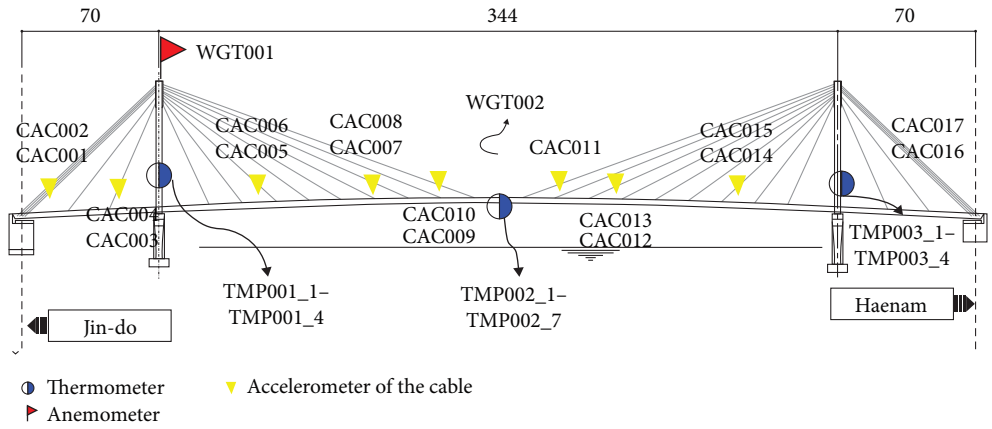

Figure 3: Location of sensors at the 2nd Jin-do bridge.

the RMS indicated scale-dependent measures. Therefore, several studies have proposed scale-independent measures [52, 53]. The MAPE indicates the accuracy or error of the prediction as a percentage and is calculated as follows [54]:

$$\text{MAPE} = \frac{100}{n}\sum_{i=1}^{n}\left|\frac{\dot{f}(\mathbf{X}_i) - y_i}{y_i}\right|, \tag{9}$$

where N denotes the number of measurement points, $\dot{f}(\mathbf{X}_i)$ denotes the predictive mean at the test input $\mathbf{X}_i$ and y_i denotes the actual measurement.

However, the MAPE can have different evaluation values for the same error. For example, if $\dot{f}(\mathbf{X}_i)$ and y_i are assumed to be 250 and 200, respectively, then the MAPE can be calculated using Equation (9) as 20%. In contrast, if $\dot{f}(\mathbf{X}_i)$ and y_i are assumed to be 200 and 250, respectively, the MAPE indicates a percentage error of 25%. In addition to the previous problem, when the measurement approaches zero (i.e., $y_i \approx 0$), the MAPE value exponentially increases the amplification of this phenomenon. In other words, the error increases rapidly when the value of the measurement (i.e., y_i) is small.

To resolve this problem with MAPE, Hyndman and Koehler [50] proposed an improved method called symmetric MAPE (sMAPE), which is expressed as follows:

$$\text{sMAPE} = \frac{100}{n}\sum_{i=1}^{n}\frac{\left|\dot{f}(\mathbf{X}_i) - y_i\right|}{\left(\left|\dot{f}(\mathbf{X}_i)\right| + |y_i|\right)/2}. \tag{10}$$

Using the sMAPE to address the previous MAPE example results in the same percentage error of ~22%. Additionally, the sMAPE error percentage does not rapidly increase when the measurement of the value is small (i.e., $y_i \approx 0$). That is, the sMAPE solves the MAPE problem. Therefore, this study adopts the sMAPE to assess the predictive mean.

Nevertheless, a problem occurs when using sMAPE when the signs of the measured and predicted values differ (i.e., one is a positive number, and the other is a negative number). Therefore, Shin et al. [54] proposed a new algorithm to compensate for the MAPE and sMAPE problems. However, the problem of having a different sign between the measurement and prediction values does not occur in this study; thus, the prediction error is calculated according to the sMAPE.

3.3. Parametric Study on Prediction Results Based on Correlation Coefficients. This paper proposes a method for feature selection based on the Z-index, which can select features according to the uniformity scale concerning the correlation of the entire input and output data, as described in Section 2. Two parametric studies are conducted using two different feature-selection methods and varying threshold values (i.e., criteria) to compare the effects of different feature-selection schemes. First, the feature selection involves ranking based on the absolute value of the correlation coefficient, and the criterion is to set constant values from 0.05 to 0.55 at 0.1 intervals. The six scenarios are listed in Table 1, where a P as the first character of a scenario number indicates that the feature selections are based on the Pearson correlation coefficient. A prediction model is constructed using GPR after the relevant input data are selected as the criteria. Four weeks of data from March 16 to April 12, 2019 are used to train the learned model. The prediction results are compared with the actual measurement data in terms of sMAPE after the learned model performs the prediction for the following week (April 12–19, 2019).

Table 1: Scenario number and associated criteria value based on correlation coefficient.

Scenario number	Criteria based on $\lvert\rho\rvert$
P1	$\lvert\rho\rvert \geq 0.05$
P2	$\lvert\rho\rvert \geq 0.15$
P3	$\lvert\rho\rvert \geq 0.25$
P4	$\lvert\rho\rvert \geq 0.35$
P5	$\lvert\rho\rvert \geq 0.45$
P6	$\lvert\rho\rvert \geq 0.55$

The correlation coefficient matrix for the 19 input and 17 output data points is shown in Figure 4. The input data consist of 15 temperatures (i.e., Temps 1–15), two wind speeds (i.e., W.S. 1 and W.S. 2), and two wind direction data points. The output data consists of 17 tension force data points (i.e., Cables 1–17). The units of these data are °C, m/s, °, and kN, respectively. Darker shades of blue in the correlation coefficient matrix indicate higher correlation coefficients. For example, the tension forces of Cables 1–4 generally exhibit high correlation levels with the most input data, particularly with Temps 5–8. In contrast, Cable 10 generally exhibits a low correlation with all input data. Cables 8, 9, 11, and 12 generally exhibit a low correlation level, but a relatively high correlation level with the wind speed data (i.e., W.S. 1 and W.S. 2) compared with those of other cables.

Based on this correlation coefficient matrix, a feature (i.e., input data) is selected for each cable that is used for predicting the tension force according to the criteria set for each scenario. Table 2 shows the feature selection and corresponding prediction results for P1–P3 (i.e., $|\rho| \geq 0.05$, $|\rho| \geq 0.15$, and $|\rho| \geq 0.25$), respectively.

First, many input data are selected overall for P1 (i.e., $|\rho| \geq 0.05$) because the criterion of feature selection is the lowest among those in all scenarios. In particular, 18 or 19 input data points are selected for Cables 1–4 which are highly correlated with most of the input data. In contrast, Cable 10 exhibits a low correlation with most of the input data, and only three input data points are selected despite the low criterion of 0.05. The running time and sMAPE values are also listed in Table 2. These values are calculated by comparing the actual measurement data with the prediction results for the week of April 12–19, 2019, using the prediction models (GPR) as executed training for the 4 weeks from March 16 to April 12, 2019. All sMAPE values are less than 1% and most cables achieve high prediction performance. However, increasing the amount of input data generally requires long execution times. The results for Scenarios P2 and P3 indicate a reduction in the selected input data (i.e., features) by

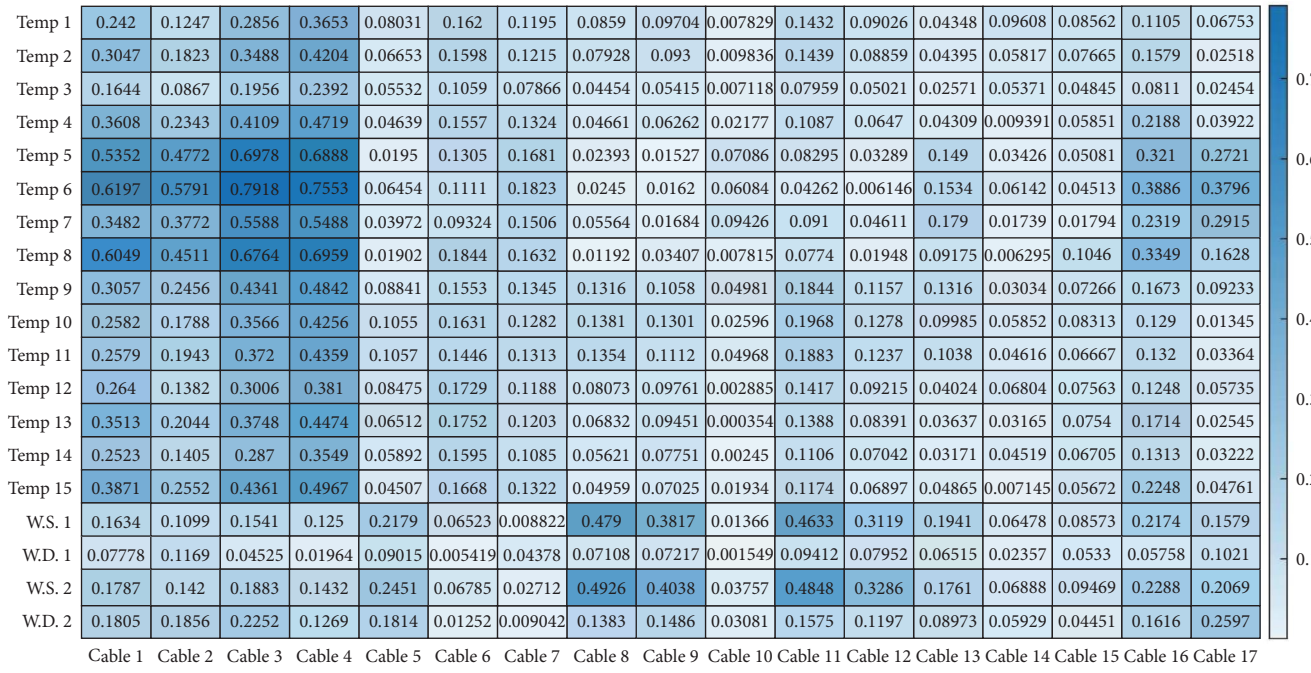

Figure 4: Correlation coefficient matrix of input and output data.

Table 2: Number of selected input data, sMAPE values, and computational times for prediction in Scenarios P1–P3.

Cable number	P1			P2			P3		
	Number of selected input data	sMAPE (%)	Time (min)	Number of selected input data	sMAPE (%)	Time (min)	Number of selected input data	sMAPE (%)	Time (min)
Cable 1	19	0.393	26.894	18	0.410	29.320	13	0.372	22.178
Cable 2	19	0.471	37.859	12	0.240	7.226	5	0.237	2.289
Cable 3	18	0.516	36.906	18	0.516	36.910	14	0.490	20.611
Cable 4	18	0.456	25.692	15	0.457	15.549	14	0.444	12.184
Cable 5	14	0.890	34.657	3	0.763	1.707	0	—	—
Cable 6	17	0.649	36.152	10	0.632	9.301	0	—	—
Cable 7	15	0.166	18.780	4	0.169	2.723	0	—	—
Cable 8	13	0.386	14.668	2	0.176	0.934	2	0.176	0.920
Cable 9	15	0.337	19.766	2	0.211	0.920	2	0.176	0.920
Cable 10	3	0.276	1.915	0	—	—	0	—	—
Cable 11	18	0.408	36.180	6	0.518	3.558	2	0.269	0.828
Cable 12	15	0.274	18.789	2	0.115	0.919	2	0.115	0.914
Cable 13	11	0.151	13.338	4	0.199	1.809	0	—	—
Cable 14	9	0.172	9.554	0	—	—	0	—	—
Cable 15	15	0.433	29.294	0	—	—	0	—	—
Cable 16	19	0.233	50.595	12	0.234	13.432	3	0.233	1.945
Cable 17	11	0.285	11.625	7	0.315	6.047	4	0.282	2.793

increasing the criterion, and the associated computational time is reduced accordingly. Meanwhile, the sMAPE for Cable 5 decreases with a decreasing number of selected input data, whereas that for Cable 13 increases. Therefore, an appropriate amount of input data must be considered for each cable for prediction, and it is impossible to determine this number using a uniform criterion based on the correlation coefficient. The results for Scenarios P4–P6 (criteria of 0.35–0.55) are listed in Table 3, and the overall results are summarized in Figure 5.

The optimal criteria based on the correlation coefficient varies for each cable, as listed in Table 4. For example, Cable 4 exhibits the best performance when using a criterion of 0.45, whereas Cable 8 exhibits the best prediction performance

Table 3: Number of selected input data, sMAPE values, and computational times for prediction in Scenarios P4–P6.

Cable number	P4			P5			P6		
	Number of selected input data	sMAPE (%)	Time (min)	Number of selected input data	sMAPE (%)	Time (min)	Number of selected input data	sMAPE (%)	Time (min)
Cable 1	6	0.384	3.414	3	0.367	1.693	2	0.418	1.019
Cable 2	4	0.250	2.207	3	0.303	1.240	1	0.412	0.518
Cable 3	10	0.401	8.224	4	0.491	2.157	4	0.491	2.165
Cable 4	14	0.444	12.373	7	0.442	3.893	3	0.475	1.529
Cable 5	0	—	—	0	—	—	0	—	—
Cable 6	0	—	—	0	—	—	0	—	—
Cable 7	0	—	—	0	—	—	0	—	—
Cable 8	2	0.176	0.928	2	0.176	0.934	0	—	—
Cable 9	2	0.211	0.927	0	—	—	0	—	—
Cable 10	0	—	—	0	—	—	0	—	—
Cable 11	2	0.269	0.839	0	—	—	0	—	—
Cable 12	0	—	—	0	—	—	0	—	—
Cable 13	0	—	—	0	—	—	0	—	—
Cable 14	—	—	—	—	—	—	—	—	—
Cable 15	0	—	—	0	—	—	0	—	—
Cable 16	1	0.197	0.468	0	—	—	0	—	—
Cable 17	1	0.301	0.556	0	—	—	0	—	—

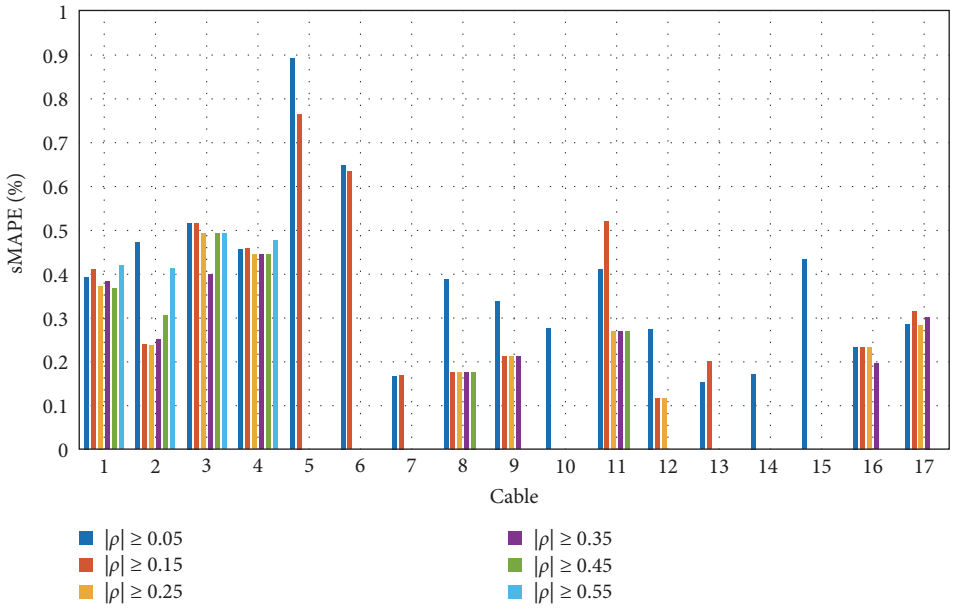

Figure 5: sMAPE of prediction results in six scenarios with varying correlation coefficient-based threshold value for Cables 1–17.

when using a criterion of 0.15. Moreover, some cables may not be predicted if the criterion is set too high because no selected features (i.e., input data) would be available for the high criterion. This demonstrates that the use of a fixed criterion based on the correlation coefficient is inefficient.

3.4. Parametric Study on Prediction Results Based on Z-Index. Feature selection is performed in this parametric study based on the Z-index, and the criteria are set to constant values from −1.5 to 1 at 0.5 intervals. Table 5 shows the six scenarios, where a "Z" as the first character of a scenario number indicates that the feature selections are based on the Z-index. A prediction model is constructed using GPR after the input data are selected. Similar to the testing done in Section 3.2, this parametric study uses 4 weeks of data for training from March 16 to April 12, 2019, and the prediction is made for the following week April 12–19, 2019. The Z-index matrix for the 19 input and 17 output data points is calculated using Equation (1) and correlation coefficients from Figure 5, as shown in Figure 6.

Table 4: Optimal criteria of cables based on correlation coefficient.

Cable number	Optimal criteria based on correlation coefficient
1	$\|\rho\| \geq 0.45$
2	$\|\rho\| \geq 0.25$
3	$\|\rho\| \geq 0.35$
4	$\|\rho\| \geq 0.45$
5	$\|\rho\| \geq 0.15$
6	$\|\rho\| \geq 0.15$
7	$\|\rho\| \geq 0.05$
8	$\|\rho\| \geq 0.15$
9	$\|\rho\| \geq 0.15$
10	$\|\rho\| \geq 0.05$
11	$\|\rho\| \geq 0.25$
12	$\|\rho\| \geq 0.25$
13	$\|\rho\| \geq 0.05$
14	$\|\rho\| \geq 0.05$
15	$\|\rho\| \geq 0.05$
16	$\|\rho\| \geq 0.35$
17	$\|\rho\| \geq 0.25$

Table 5: Scenario number and associated criteria based on Z-index.

Scenario number	Criteria value based on Z-index
Z1	$z \geq -1.5$
Z2	$z \geq -1$
Z3	$z \geq -0.5$
Z4	$z \geq 0$
Z5	$z \geq 0.5$
Z6	$z \geq 1$

One noteworthy point for the matrix in Figure 6 is that the Z-index values are relatively uniformly distributed, compared with those of the matrix in Figure 4. This indicates that the values are normalized by introducing the Z-score. Based on this Z-index matrix, features (i.e., input data) are selected according to the criteria for each scenario to predict the tension force of each cable. The results for Scenarios Z1–Z6 (i.e., criteria of −1.5 to 1) are shown in Tables 6 and 7 and the overall results are summarized in Figure 7. The numbers of selected input data are similar to each other, unlike the previous parametric study based on the correlation coefficient, as shown in Tables 6 and 7. In addition, each cable has a similar running time, which was realized by introducing the Z-index.

Furthermore, the variations in sMAPE according to the Z-index are shown in Figure 8(a). Z5 (Z-index of 0.5) and Z6 (Z-index of 1) exhibit the lowest errors compared to those of Z1–Z4. The minimum-error predictions for the 17 cables are shown in Figure 8(b). It is noteworthy that Scenario Z5 shows the minimum prediction errors for more cables than those in the other scenarios. Therefore, in this example, the optimal Z-index-based criterion for feature selection (input data) is determined to be 0.5.

4. Results of Probabilistic Response Prediction

The ability of the proposed method to improve prediction is confirmed by selecting the optimal input data. The results for Cables 1 and 2 following Scenario Z5 using the proposed method and optimal results from Section 3 are shown in Figures 9(a) and 9(b), respectively. The measurement data (i.e., training data and test data), predictive mean, and 95% prediction intervals are denoted as black dots, a blue line, and a gray area, respectively. The confidence interval level can be set differently depending on the criteria that are the focus of the user. Additionally, measurement data corresponding to a duration of 4 weeks (March 16 to April 12, 2019) are utilized to establish the GPR. However, Figures 9(a) and 9(b) depict 3 days of training data to clearly show the prediction results. The prediction results are compared with the actual measurement data after the constructed GPR performed the prediction for the following week (April 13 to April 19, 2019). The data points are classified as abnormal if the test (actual measurement) data from points April 13 to April 19, 2019, deviated significantly from the 95% predicted interval, as shown in Figure 9. Therefore, it is possible to establish a threshold for anomaly detection and assess the structural condition of the cable system in real-time by utilizing the prediction results. The proposed method is expected to produce more accurate and efficient prediction results, thereby enabling the operation and maintenance of structures.

Figure 10 shows the predictive means and 95% prediction intervals of tension forces for representatively selected cables, and it is observed that most of the actual data are located within the confidence intervals. Therefore, the proposed method provides accurate predictive means and prediction interval results overall. For example, the tension forces of Cables 1 and 2 fluctuate smoothly with a relatively constant cycle, and in these cases, the prediction results also fluctuate smoothly with a relatively small confidence interval. On the other hand, the tension forces of Cables 5 and 7 dramatically change in certain ranges. In these cases, the prediction results still show good agreement with the actual measurement (i.e., test data), but it is also observed that the overall confidence interval of the prediction results is wide due to irregular fluctuations in the measurement data. In the case of Cable 12; however, the predictive confidence interval is wide even though the test data continues to maintain a certain level without significant fluctuations. This is thought to be due to a numerical problem induced by a low correlation coefficient of the cable with the other cables, which can be a limitation of the proposed method. Some other researchers suggested making data-driven predictions considering the correlation coefficient between outputs. It is thought that the proposed method can be improved when it considers multioutput correlation in addition to input–output correlation, because in the case of a complex structural system such as a cable-stayed bridge, the tension forces of cables may be highly correlated. However, the predictive mean provided by the proposed method still shows good agreement with the test data. In conclusion, the proposed method provides accurate predictive means and prediction interval results, and immediate

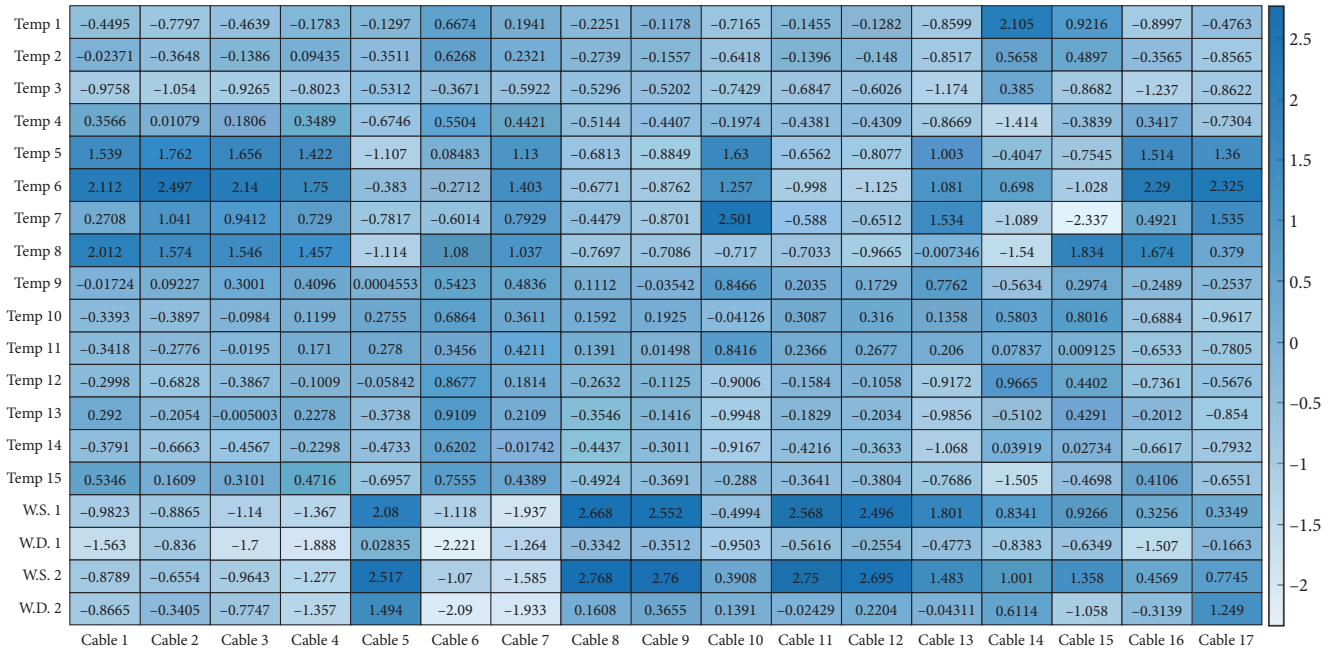

Figure 6: Z-index matrix of input and output data.

Table 6: Number of selected input data, sMAPE values, and computational times for prediction in Scenarios Z1–Z3.

Cable number	Z1			Z2			Z3		
	Number of selected input data	sMAPE (%)	Time (min)	Number of selected input data	sMAPE (%)	Time (min)	Number of selected input data	sMAPE (%)	Time (min)
Cable 1	18	0.410	38.680	18	0.410	38.708	14	0.370	27.106
Cable 2	19	0.471	49.813	18	0.473	53.968	12	0.240	9.618
Cable 3	18	0.516	48.808	17	0.516	40.298	14	0.490	27.160
Cable 4	18	0.456	33.900	15	0.457	20.591	14	0.444	16.164
Cable 5	19	0.918	74.711	17	0.885	43.998	13	0.896	28.766
Cable 6	17	0.649	47.555	15	0.649	42.080	14	0.666	24.234
Cable 7	16	0.167	35.730	15	0.166	24.694	14	0.174	38.301
Cable 8	19	0.499	39.730	19	0.499	39.493	14	0.386	31.504
Cable 9	19	0.335	44.947	19	0.335	44.749	14	0.347	22.482
Cable 10	19	0.244	35.710	19	0.244	35.586	11	0.277	19.246
Cable 11	19	0.422	38.476	19	0.422	38.425	13	0.353	14.609
Cable 12	19	0.298	22.751	18	0.294	40.293	14	0.277	25.594
Cable 13	19	0.174	47.143	17	0.146	32.699	11	0.151	17.751
Cable 14	17	0.167	47.608	15	0.170	31.275	12	0.171	21.887
Cable 15	18	0.429	36.201	16	0.429	44.307	13	0.432	34.108
Cable 16	18	0.238	30.645	17	0.238	36.072	12	0.234	17.806
Cable 17	19	0.297	45.870	19	0.297	45.723	10	0.285	14.256

management of the structure or sensor fault should be conducted if the measurement data deviates continuously from the prediction interval, as this would be considered an abnormal response.

5. Conclusions

This study proposed a data-driven method for predicting the probabilistic response of cable-stayed bridges. The objective was to effectively predict the tension force of the cables by constructing an optimal prediction model based on the Z-index. This method improved the accuracy and efficiency of the prediction model while considering the correlation between the environmental data and cables. The proposed method was comprised of two steps. The first step was feature selection for the decision of an optimal criterion based on the Z-index, and the second step was the construction of a prediction model by employing GPR. The best input data

Table 7: Number of used input data, sMAPE values, and computational times for prediction in Scenario Z4–Z6.

Cable number	Z4			Z5			Z6		
	Number of selected input data	sMAPE (%)	Time (min)	Number of selected input data	sMAPE (%)	Time (min)	Number of selected input data	sMAPE (%)	Time (min)
Cable 1	7	0.333	6.049	4	0.403	2.854	3	0.367	2.220
Cable 2	7	0.293	8.383	4	0.250	2.856	4	0.250	2.885
Cable 3	7	0.430	5.693	4	0.491	2.744	3	0.547	2.113
Cable 4	11	0.423	10.286	4	0.403	2.852	3	0.475	1.934
Cable 5	7	0.900	7.568	3	0.763	2.195	3	0.763	2.202
Cable 6	12	0.649	24.671	10	0.632	12.273	1	0.577	0.593
Cable 7	13	0.174	27.281	4	0.169	3.504	3	0.199	2.661
Cable 8	6	0.314	6.748	2	0.176	1.172	2	0.176	1.181
Cable 9	5	0.280	3.609	2	0.211	1.171	2	0.211	1.174
Cable 10	7	0.283	8.702	5	0.314	4.788	3	0.276	2.473
Cable 11	5	0.518	4.860	2	0.269	1.059	2	0.269	1.062
Cable 12	6	0.179	6.831	2	0.115	1.169	2	0.115	1.177
Cable 13	8	0.153	8.196	6	0.212	4.482	5	0.173	3.986
Cable 14	11	0.172	19.236	8	0.173	8.812	2	0.171	1.394
Cable 15	11	0.452	22.352	5	0.359	5.923	2	0.366	0.921
Cable 16	8	0.224	10.158	3	0.233	2.500	3	0.233	2.517
Cable 17	7	0.315	7.845	5	0.292	3.526	4	0.282	3.640

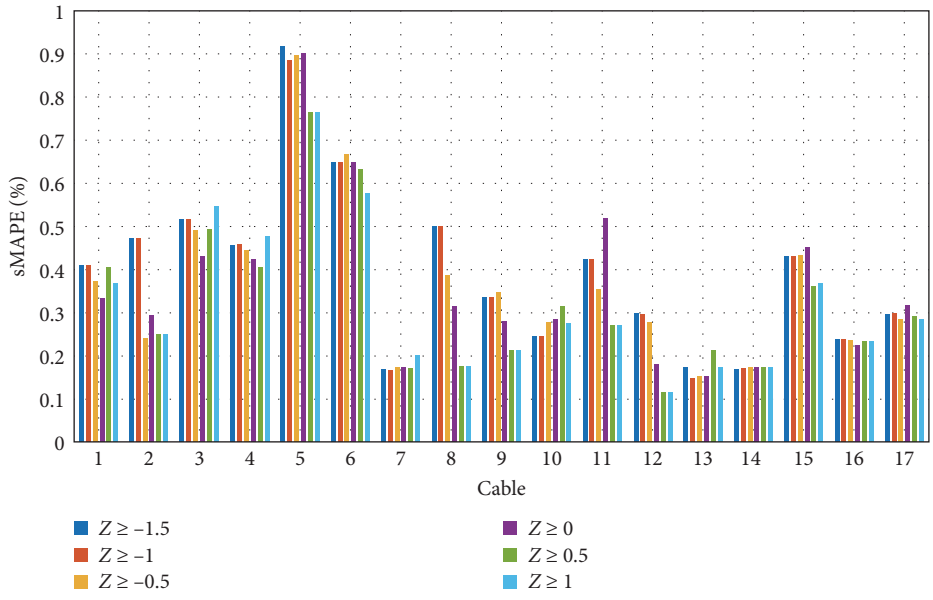

Figure 7: sMAPE of prediction results in six scenarios with varying Z-index-based threshold value for Cables 1–17.

were determined through feature selection based on the Z-index according to an optimal criterion. Additionally, the accuracy of the prediction model was improved while reducing running time. A probabilistic model was constructed using GPR after selecting the input data according to the proposed feature selection, considering the uncertainty of the data and the machine-learning model. The standard deviation and predictive mean of the tension force were provided, and the GPR results were used to assess the stationary state of stayed cables in comparison with the obtained measurement data. The proposed method was applied to an application example that utilized measurement data from various sensors deployed on the 2nd Jin-do Bridge, an actual cable-stayed bridge in the Republic of Korea. Two parametric studies were performed using two different feature-selection methods based on the correlation coefficient and Z-index to compare

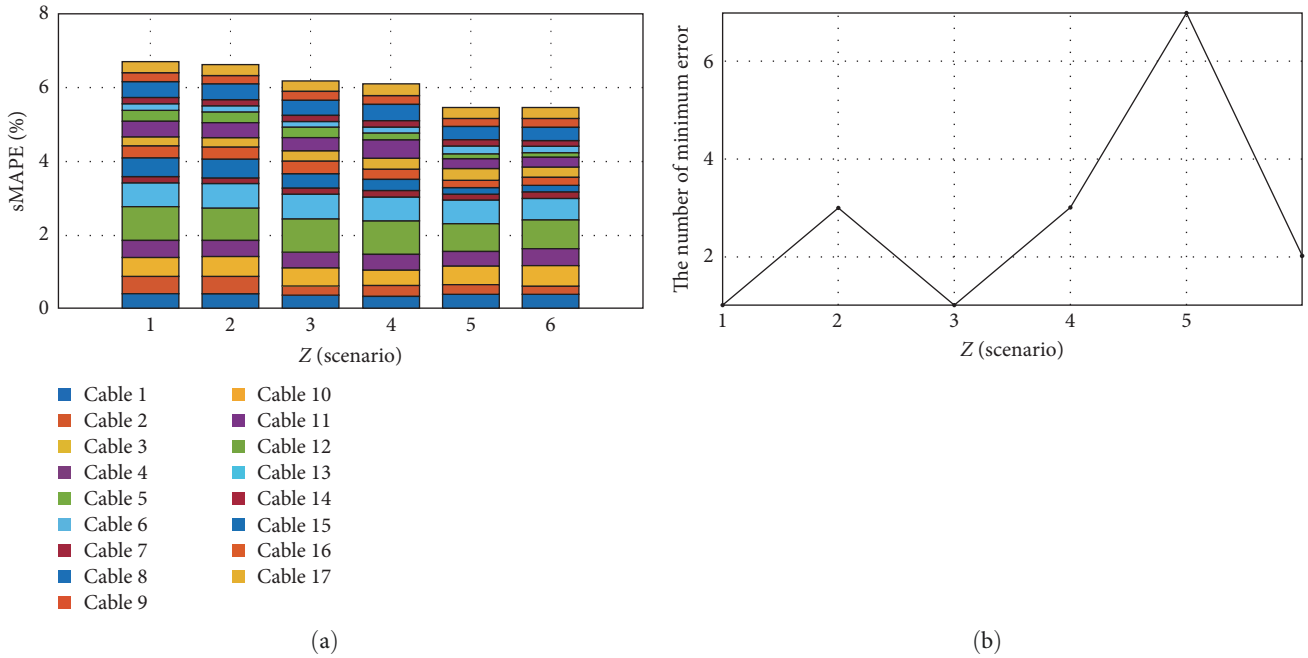

(a) (b)

FIGURE 8: (a) Results of the cumulative value and sMAPE in Scenarios Z1–Z6 and (b) number of minimum error predictions in Scenarios Z1–Z6.

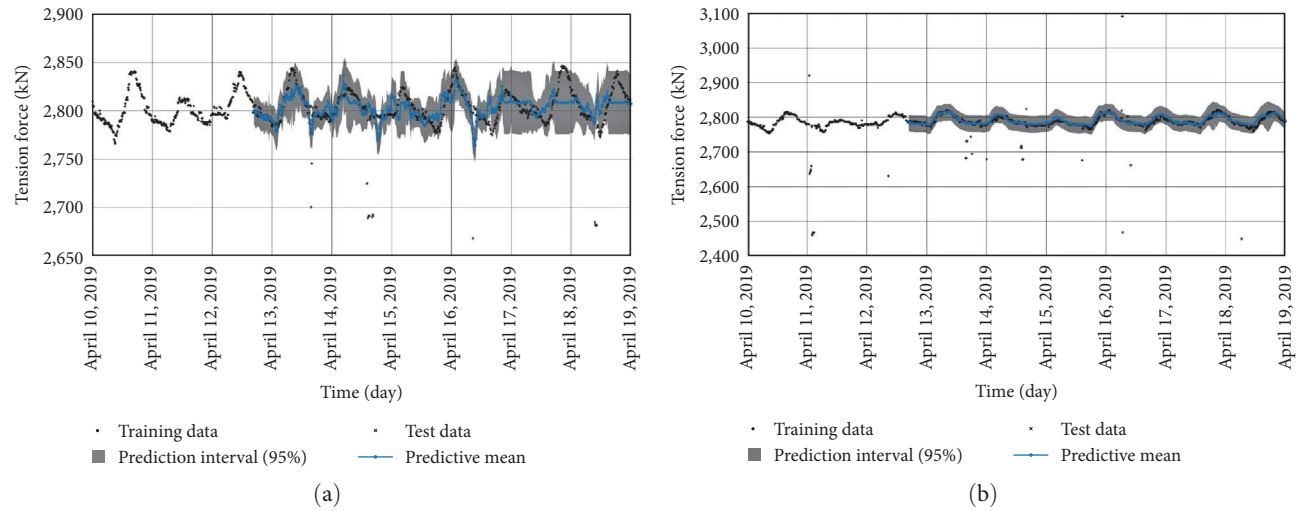

(a) (b)

FIGURE 9: (a) Prediction results (predictive mean and confidence interval) and measurement data following Scenario Z5 for Cables: (a) 1 and (b) 2.

the effects of different feature-selection schemes. Consequently, it was observed that an optimal feature selection criterion could be determined based on the Z-index. This was because the Z-index values were uniformly distributed, in contrast with the correlation coefficient matrix. Subsequently, the prediction results from the GPR exhibited highly accurate results after the input features were selected using the optimal criterion, despite reducing the computational cost.

It was also observed that the prediction results were less accurate for a few cables with relatively low correlation coefficients between the input and output data, which could be the limitation of the proposed method. However, some other researchers suggested making data-driven predictions considering the correlation coefficient between outputs. It is thought that the proposed method can be improved when it considers multi-output correlation in addition to input–output correlation,

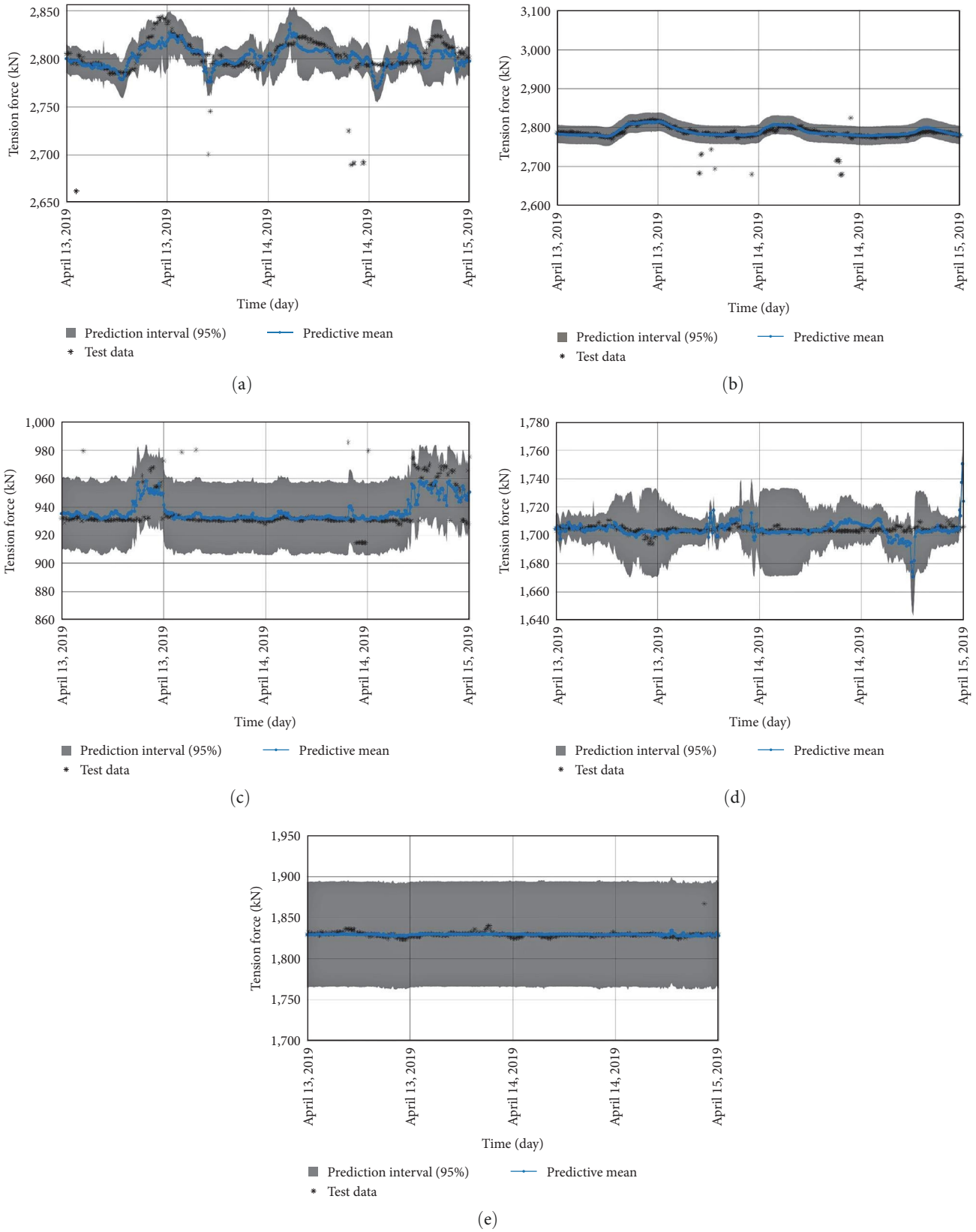

Figure 10: Predictive means and 95% prediction intervals of tension forces for selected cables: (a) Cable 1, (b) Cable 2, (c) Cable 5, (d) Cable 7, and (e) Cable 12.

because in the case of a complex structural system such as a cable-stayed bridge, the tension forces of cables may be highly correlated.

Data Availability

The data that support the findings of this study are available from Korea Authority of Land & Infrastructure Safety. Restrictions apply to the availability of these data, which were used under license for this study. Data are available from the author(s) with the permission of Korea Authority of Land & Infrastructure Safety.

Conflicts of Interest

The authors declare that there are no conflicts of interest regarding the publication of this article.

Acknowledgments

This work was supported by the National Research Foundation of Korea (NRF) grant funded by the Korea Government (MSIT) (No. RS-2022-00144434). In addition, the authors appreciate Korea Authority of Land & Infrastructure Safety (KALIS) on providing the data used in this study.

References

[1] M. Gatti, "Structural health monitoring of an operational bridge: a case study," *Engineering Structures*, vol. 195, pp. 200–209, 2019.

[2] M. Liu, D. M. Frangopol, and S. Kim, "Bridge system performance assessment from structural health monitoring: a case study," *Journal of Structural Engineering*, vol. 135, no. 6, pp. 733–742, 2009.

[3] D. Agdas, J. A. Rice, J. R. Martinez, and I. R. Lasa, "Comparison of visual inspection and structural-health monitoring as bridge condition assessment methods," *Journal of Performance of Constructed Facilities*, vol. 30, no. 3, Article ID 04015049, 2016.

[4] S. Jang, H. Jo, S. Cho et al., "Structural health monitoring of a cable-stayed bridge using smart sensor technology: deployment and evaluation," *Smart Structures and Systems*, vol. 6, no. 5_6, pp. 439–459, 2010.

[5] S.-H. Sim, J. Li, H. Jo et al., "A wireless smart sensor network for automated monitoring of cable tension," *Smart Materials and Structures*, vol. 23, no. 2, Article ID 025006, 2013.

[6] S. Sharma, S. K. Dangi, S. K. Bairwa, and S. Sen, "Comparative study on sensitivity of acceleration and strain responses for bridge health monitoring," *Journal of Structural Integrity and Maintenance*, vol. 7, no. 4, pp. 238–251, 2022.

[7] S. E. Haji Agha Mohammad Zarbaf, M. Norouzi, R. J. Allemang, V. J. Hunt, and A. Helmicki, "Stay cable tension estimation of cable-stayed bridges using genetic algorithm and particle swarm optimization," *Journal of Bridge Engineering*, vol. 22, no. 10, Article ID 05017008, 2017.

[8] V. Chandola, A. Banerjee, and V. Kumar, "Anomaly detection: a survey," *ACM Computing Surveys*, vol. 41, no. 3, pp. 1–58, 2009.

[9] T.-H. Yi, H.-B. Huang, and H.-N. Li, "Development of sensor validation methodologies for structural health monitoring: a comprehensive review," *Measurement*, vol. 109, pp. 200–214, 2017.

[10] T.-C. Huynh, J.-H. Park, and J.-T. Kim, "Structural identification of cable-stayed bridge under back-to-back typhoons by wireless vibration monitoring," *Measurement*, vol. 88, pp. 385–401, 2016.

[11] A. B. Mehrabi and S. Farhangdoust, "A laser-based noncontact vibration technique for health monitoring of structural cables: background, success, and new developments," *Advances in Acoustics and Vibration*, vol. 2018, Article ID 8640674, 13 pages, 2018.

[12] M. Ju, C. Park, and G. Kim, "Structural Health Monitoring (SHM) for a cable stayed bridge under typhoon," *KSCE Journal of Civil Engineering*, vol. 19, no. 4, pp. 1058–1068, 2015.

[13] S. Li, H. Li, Y. Liu, C. Lan, W. Zhou, and J. Ou, "SMC structural health monitoring benchmark problem using monitored data from an actual cable-stayed bridge," *Structural Control and Health Monitoring*, vol. 21, no. 2, pp. 156–172, 2014.

[14] M. R. Kaloop and J. W. Hu, "Stayed-cable bridge damage detection and localization based on accelerometer health monitoring measurements," *Shock and Vibration*, vol. 2015, Article ID 102680, 11 pages, 2015.

[15] D.-H. Yang, H.-L. Gu, T.-H. Yi, and H.-N. Li, "Bridge cable anomaly detection based on local variability in feature vector of monitoring group cable forces," *Journal of Bridge Engineering*, vol. 28, no. 6, Article ID 04023030, 2023.

[16] Y. Lee, W.-J. Park, Y.-J. Kang, and S. Kim, "Response pattern analysis-based structural health monitoring of cable-stayed bridges," *Structural Control and Health Monitoring*, vol. 28, no. 11, Article ID e2822, 2021.

[17] A. P. Pamuncak, M. R. Salami, A. Adha, B. Budiono, and I. Laory, "Estimation of structural response using convolutional neural network: application to the Suramadu bridge," *Engineering Computations*, vol. 38, no. 10, pp. 4047–4065, 2021.

[18] F. T. Ni, J. Zhang, and M. N. Noori, "Deep learning for data anomaly detection and data compression of a long-span suspension bridge," *Computer-Aided Civil and Infrastructure Engineering*, vol. 35, no. 7, pp. 685–700, 2020.

[19] Y. Deng, M. Zhang, D.-M. Feng, and A.-Q. Li, "Predicting fatigue damage of highway suspension bridge hangers using weigh-in-motion data and machine learning," *Structure and Infrastructure Engineering*, vol. 17, no. 2, pp. 233–248, 2021.

[20] X.-W. Ye, Z. Sun, and J. Lu, "Prediction and early warning of wind-induced girder and tower vibration in cable-stayed bridges with machine learning-based approach," *Engineering Structures*, vol. 275, Part A, Article ID 115261, 2023.

[21] A. Kendall and Y. Gal, "What uncertainties do we need in bayesian deep learning for computer vision?" in *Proceedings of the 31st International Conference on Neural Information Processing Systems*, pp. 5580–5590, Curran Associates Inc., Long Beach, California, USA, December 2017.

[22] J. Lee, K.-C. Lee, and Y.-J. Lee, "Long-term deflection prediction from computer vision-measured data history for high-speed railway bridges," *Sensors*, vol. 18, no. 5, Article ID 1488, 2018.

[23] Q.-A. Wang, C. Zhang, Z.-G. Ma, and Y.-Q. Ni, "Modelling and forecasting of SHM strain measurement for a large-scale suspension bridge during typhoon events using variational heteroscedastic Gaussian process," *Engineering Structures*, vol. 251, Article ID 113554, 2022.

[24] *Subspace, Latent Structure and Feature Selection: Statistical and Optimization Perspectives Workshop, SLSFS 2005 Bohinj, Slovenia, February 23–25, 2005, Revised Selected Papers*, Vol. 3940, Springer Berlin, Heidelberg, 2005.

[25] J. Cai, J. Luo, S. Wang, and S. Yang, "Feature selection in machine learning: a new perspective," *Neurocomputing*, vol. 300, pp. 70–79, 2018.

[26] Z. Zhao, F. Morstatter, S. Sharma, S. Alelyani, A. Anand, and H. Liu, *Advancing Feature Selection Research-ASU Feature Selection Repository*, Arizona State University, Tempe, Arizona, 2010.

[27] A. L. Blum and P. Langley, "Selection of relevant features and examples in machine learning," *Artificial Intelligence*, vol. 97, no. 1-2, pp. 245–271, 1997.

[28] D. Mladenić, "Feature selection for dimensionality reduction," in *Subspace, Latent Structure and Feature Selection*, pp. 84–102, Springer, Berlin, Heidelberg, Bohinj, Slovenia, Berlin Heidelberg, 2006.

[29] R. Ghiasi and A. Malekjafarian, "Feature subset selection in structural health monitoring data using an advanced binary slime mould algorithm," *Journal of Structural Integrity and Maintenance*, vol. 8, no. 4, pp. 209–225, 2023.

[30] I. Inza, P. Larrañaga, R. Blanco, and A. J. Cerrolaza, "Filter versus wrapper gene selection approaches in DNA microarray domains," *Artificial Intelligence in Medicine*, vol. 31, no. 2, pp. 91–103, 2004.

[31] S. Das, "Filters, wrappers and a boosting-based hybrid for feature selection," in *Proceedings of the Eighteenth International Conference on Machine Learning*, pp. 74–81, Morgan Kaufmann Publishers Inc., June 2001.

[32] X.-Y. Liu, Y. Liang, S. Wang, Z.-Y. Yang, and H.-S. Ye, "A hybrid genetic algorithm with wrapper-embedded approaches for feature selection," *IEEE Access*, vol. 6, pp. 22863–22874, 2018.

[33] M. Sebban and R. Nock, "A hybrid filter/wrapper approach of feature selection using information theory," *Pattern Recognition*, vol. 35, no. 4, pp. 835–846, 2002.

[34] C. Ding and H. Peng, "Minimum redundancy feature selection from microarray gene expression data," *Journal of Bioinformatics and Computational Biology*, vol. 3, no. 2, pp. 185–205, 2005.

[35] H.-H. Hsu, C.-W. Hsieh, and M.-D. Lu, "Hybrid feature selection by combining filters and wrappers," *Expert Systems with Applications*, vol. 38, no. 7, pp. 8144–8150, 2011.

[36] C. Fang, H. Tang, Y. Li, and J. Zhang, "Stochastic response of a cable-stayed bridge under non-stationary winds and waves using different surrogate models," *Ocean Engineering*, vol. 199, Article ID 106967, 2020.

[37] S. Khalid, T. Khalil, and S. Nasreen, "A survey of feature selection and feature extraction techniques in machine learning," in *2014 Science and Information Conference*, pp. 372–378, IEEE, London, UK, August 2014.

[38] C. Cheadle, M. P. Vawter, W. J. Freed, and K. G. Becker, "Analysis of microarray data using Z score transformation," *The Journal of Molecular Diagnostics*, vol. 5, no. 2, pp. 73–81, 2003.

[39] S. Kappal, "Data normalization using median median absolute deviation MMAD based Z-score for robust predictions vs. min–max normalization," *London Journal of Research in Science: Natural and Formal*, vol. 19, no. 4, 2019.

[40] S. Gopal Krishna Patro and K. K. Sahu, "Normalization: a preprocessing stage," 2015.

[41] C. Saranya and G. Manikandan, "A study on normalization techniques for privacy preserving data mining," *International Journal of Engineering and Technology*, vol. 5, no. 3, pp. 2701–2704, 2013.

[42] C. E. Rasmussen, "Gaussian processes in machine learning," in *Summer School on Machine Learning*, pp. 63–71, Springer, Berlin, Heidelberg, 2003.

[43] Z. Zhang, L. Ye, H. Qin et al., "Wind speed prediction method using shared weight long short-term memory network and Gaussian process regression," *Applied Energy*, vol. 247, pp. 270–284, 2019.

[44] K. Liu, Y. Li, X. Hu, M. Lucu, and W. D. Widanage, "Gaussian process regression with automatic relevance determination kernel for calendar aging prediction of lithium-ion batteries," *IEEE Transactions on Industrial Informatics*, vol. 16, no. 6, pp. 3767–3777, 2019.

[45] P. Asadollahi and J. Li, "Statistical analysis of modal properties of a cable-stayed bridge through long-term wireless structural health monitoring," *Journal of Bridge Engineering*, vol. 22, no. 9, Article ID 04017051, 2017.

[46] D. Yang, D. Youliang, and L. Aiqun, "Structural condition assessment of long-span suspension bridges using long-term monitoring data," *Earthquake Engineering and Engineering Vibration*, vol. 9, no. 1, pp. 123–131, 2010.

[47] A. Fenerci, O. Øiseth, and A. Rønnquist, "Long-term monitoring of wind field characteristics and dynamic response of a long-span suspension bridge in complex terrain," *Engineering Structures*, vol. 147, pp. 269–284, 2017.

[48] H. Zui, T. Shinke, and Y. Namita, "Practical formulas for estimation of cable tension by vibration method," *Journal of Structural Engineering*, vol. 122, no. 6, pp. 651–656, 1996.

[49] H. Nam and N. T. Nghia, "Estimation of cable tension using system identification technique: 2. experiments and applications," *KSCE Journal of Civil and Environmental Engineering Research*, vol. 25, no. 4A, pp. 669–675, 2005.

[50] R. J. Hyndman and A. B. Koehler, "Another look at measures of forecast accuracy," *International Journal of Forecasting*, vol. 22, no. 4, pp. 679–688, 2006.

[51] S. Kim and H. Kim, "A new metric of absolute percentage error for intermittent demand forecasts," *International Journal of Forecasting*, vol. 32, no. 3, pp. 669–679, 2016.

[52] C. Chatfield, "Apples, oranges and mean square," *International Journal of Forecasting*, vol. 4, no. 4, pp. 515–518, 1988.

[53] R. Fildes and S. Makridakis, "Forecasting and loss functions," *International Journal of Forecasting*, vol. 4, no. 4, pp. 545–550, 1988.

[54] K. H. Shin, C. Kim, S. H. Nam, S. J. Park, and S. S. Yoo, "Estimation method of predicted time series data based on absolute maximum value," *Journal of Energy Engineering*, vol. 27, no. 4, pp. 103–110, 2018.